Int. J. Multiphase Flow Vol. 15, No. 4, pp. 521–530, 1989
Printed in Great Britain.

0301-9322/89 $3.00 + 0.00

PARALLEL-WIRE PROBES FOR MEASUREMENT OF THICK LIQUID FILMS

J. E. KOSKIE, I. MUDAWAR and W. G. TIEDERMAN
Boiling and Two-phase Flow Laboratory, School of Mechanical Engineering, Purdue University, West Lafayette, IN 47907, U.S.A.

(*Received* 6 *July* 1988; *in revised form* 25 *January* 1989)

Abstract—A method of calibration for parallel-wire film thickness probes is presented. This method allows calibration of probes made of fine wires with dimensions that are comparable to standard machining tolerances. The resulting probes yield accurate and continuous measurements of film thickness for thick (> 1 mm) films.

Key Words: liquid films, film thickness, waves, measurement techniques

1. INTRODUCTION

The thickness of liquid films encountered in various types of process equipment has a major influence on the heat and mass transfer characteristics of these devices. Precise knowledge of the film thickness is complicated by the fact that in many flows of practical interest, such as annular two-phase flow and falling films, the interface of the film is disturbed by complex waves. Consequently, a probe designed to measure the instantaneous film thickness must accurately measure localized, small-amplitude, high-speed disturbances.

A large number of film thickness measurement techniques have been used with varying success. One method that has been particularly popular is the conductance technique, which was briefly reviewed by Hewitt (1978). All conductance probes have a basic relationship between the thickness of a liquid film and the electrical resistance between two electrodes that depends upon the location of the electrodes relative to the film. A number of electrode geometries have been utilized. Numerous investigators have used a probe that consisted of two electrodes flush-mounted in the surface over which the film is formed. Coney (1973) theoretically analyzed and experimentally tested conductivity probes consisting of two parallel rectangular strips in either a flat surface or aligned with the axis of curvature on a cylindrical surface. From his results it can be inferred that flush-mounted probes have excellent spatial resolution and thickness resolution for measurements of the order of $\leqslant 2$ mm, but suffer loss of resolution for thicker films.

By changing the form of the electrodes to parallel wires mounted normal to the wall, it is possible to greatly increase the range of film thickness over which the instrument is useful. A probe of this form was first used by Swanson (1966) and later by Miya *et al.* (1971). Brown *et al.* (1978) theoretically estimated the response of the parallel-wire probe to a square wave disturbance in a film. The present paper presents an analysis to estimate the spatial resolution in the flow direction, describes a method for *in situ* calibration of very small parallel-wire probes to prevent errors due to construction tolerances and compares the parallel-wire probes to needle-contact probes, which is another method for measuring large film thicknesses.

2. THEORETICAL ANALYSIS

The probe is constructed of two thin parallel wires stretched through the film normal to the wall over which the film flows. The wires are anchored in an insulating material at the wall, and are maintained in tension from outside the film. Wire spacing is controlled by passing the wires through accurately positioned holes in the insulating mounts. The plane containing the wires is normal to the flow.

In order to model the spatial resolution of the probe in the flow direction, it is necessary to determine the volume of liquid which contributes significantly to the resistance between the wires.

Within this region, hereafter called the probe area, the film thickness is spatially averaged. As a result of this averaging, any disturbance of the film contained within the probe area cannot be detected accurately. The following theoretical model was derived in order to determine the size of this region.

For regions that are small in comparison to the wavelength of an oscillating electromagnetic field, the electromagnetic field can be approximated as time invariant. Using this approximation it can be shown that the resistance, R, within a particular region can be determined by the volume integral of the square of the magnitude of the electromagnetic force vector (Jackson 1975):

$$R = \frac{1}{I^2} \int_v \sigma |\mathbf{E}|^2 \, d^3x, \qquad [1]$$

where σ is the conductivity of the liquid, $\mathbf{E}$ is the local electromagnetic force (e.m.f.) vector and I is the total current between the wires. When σ is a constant, the ratio of the resistance concentrated in any subregion to total resistance is independent of the ratio σ/I^2.

The size of the probe volume can be determined using [1]. By evaluating the integral over small subregions outside the wires and comparing the resistance in each to the total, it is possible to determine where the resistance is concentrated. The electrical resistance in the wires is assumed to be negligible compared to that of the liquid between the wires; therefore, the wires are assumed to be equipotential surfaces. Furthermore, it is assumed that between the wires all the electric current flows through the liquid rather than through the surrounding air. In addition, the conductivity of the liquid is assumed to be uniform and constant. Finally, three-dimensional effects of the electric field at the interfaces are neglected, and the wires are assumed to be exactly parallel and normal to the wall. Description of the electric field is therefore reduced to an area integral in planes normal to the wires.

The electrical field is the sum of the electrical fields of a point source and point sink each of magnitude λ placed a distance, a, along the x-axis of a cartesian coordinate system so that they are symmetric about the origin. The potential, Φ, of this field is given by

$$\Phi = \left(\frac{\lambda}{4\pi\xi}\right) \ln \left\{\frac{[(x-a)^2 + y^2]^{1/2}}{[(x+a)^2 + y^2]^{1/2}}\right\}, \qquad [2]$$

where ξ is the permittivity of free space. Lines of constant potential given by [2] are pairs of circles whose centers move outward along the x-axis. In a plane parallel to the wall, the wires are circles of constant potential along the x-axis with a diameter, d, each centered a distance, b, from the origin. By matching the constant potential circles that correspond to the surface of the wires with the equipotential circles for the source–sink problem one can solve for the field of the probe. In particular, given b and d, the value of the distance, a, becomes

$$a = (b^2 - d^2)^{1/2}. \qquad [3]$$

The magnitude of the e.m.f. vector $\mathbf{E}$ required in [1] is the gradient of the potential given by [2]. Evaluating this gradient and squaring its magnitude gives

$$|\mathbf{E}|^2 = |\nabla\Phi|^2 = \left(\frac{\lambda}{4\pi\xi}\right)^2 [f_1(x,y) + f_2(x,y)], \qquad [4]$$

where

$$f_1(x,y) = \left[\frac{(x-a)}{(x-a)^2 + y^2} - \frac{(x+a)}{(x+a)^2 + y^2}\right]^2 \qquad [5]$$

and

$$f_2(x,y) = y^2\left[\frac{1}{(x-a)^2 + y^2} - \frac{1}{(x+a)^2 + y^2}\right]^2. \qquad [6]$$

A numerical analysis of [1] was performed to find the region about the wires that contributed 90–99% of the total resistance between the wires. This analysis compared the integral over small regions about the wires to a numerical approximation of the integral over the entire, x, y-plane. Regions of equal contribution to total resistance are ovals; however, to simplify computation,

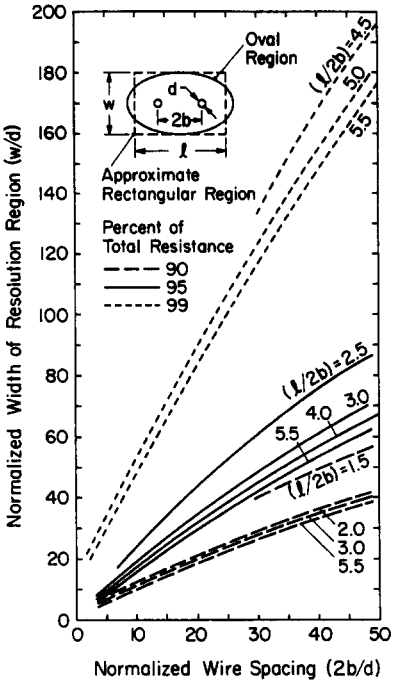

Figure 1. Resolution region of the probe as a function of wire spacing.

rectangular regions were used for the integration domain. Figure 1 shows the size of rectangles that approximate the oval region containing 90, 95 and 99% of the total resistance. Since the longer axis of the oval lies along the x-axis, the analysis consisted of fixing the length of the rectangles on the x-axis then calculating the corresponding width in the flow direction which is along the y-axis. Figure 1 also shows the oval region for a given percentage of total resistance and the approximate rectangular region which gives the same resistance. If the chosen length of the rectangle on the x-axis is too small, it is impossible to find a corresponding value for the width of the rectangle. This limit appears on the plots as incomplete curves, such as the curve for $1/2b$ of 1.5 for 90% resolution. Additionally, for rectangles with an x-axis width greater than the best approximation, the y-axis width is only slightly less than that of the best approximation, since the extended regions along the x-axis contribute little to the total integral. To make the results of the calculations universal, all distances are normalized by the wire diameter, d.

The most important conclusion that is apparent from figure 1 is that reducing the wire spacing improves the spatial resolution. This result was verified by performing calculations with the model of Brown *et al.*, which showed that reducing the wire spacing improved the response of the probe to a square wave.

The prototype probe which is described in section 4 of this paper had a dimensionless spacing $2b/d$ of 6.67. Referring to figure 1, it can be seen that 95% of the resistance is contained in a region that has a width w/D on the y-axis of approx. 14 and a length three times the wire spacing on the x-axis. Note that a longer length on the x-axis gives nearly the same width on the y-axis, so it is assumed that $1/2b = 3$ gives the shortest rectangle that accurately approximates the region containing 95% of the resistance.

3. CONSIDERATIONS IN PROBE CONSTRUCTION

The choice of wire diameters is critical to the success of the probe. The wire diameter must be sufficiently large to minimize the electrical resistance with respect to the liquid; however, it must be small enough that it does not disturb the liquid flow. Two fluid effects govern the choice of wire diameter. First, the wires must be small enough that the wake produced by the wires is negligible. Second, interfacial phenomena must be negligible.

Vortex shedding is an important consideration in wake formation. If the wires begin to shed alternating vortices, they tend to vibrate normal to the flow. Since the resistance varies with distance between the wires, this vibration causes fluctuations in resistance. Coherent vortex shedding, which is most likely to vibrate the wires, occurs when the Reynolds number based on the wire diameter is in the range $40 < Re_d < 150$ (Daily & Harleman 1966). Either this range should be avoided or the natural frequency of the wires should be moved to frequencies outside this range by changing the tension in the wires. The result of wire vibration is noise in the output signal. If the wires are stretched with sufficient tension that the natural frequencies of vibration are much higher than any frequency expected in the the data signal, the noise induced by wire vibration can be eliminated by filtering the signal.

There are three types of interfacial phenomena that could influence the performance of the probe. Surface tension will cause the formation of the meniscus on the wires. Visual inspection of the meniscus on the static test probe demonstrated that its height was smaller than the diameter of the wires. No method was available to measure the meniscus on the wires with a vertical falling film. Bow waves and wakes could also influence the probe output. Still photography revealed that a small bow wave existed downstream of the probe which precluded alignment of several two-wire probes at the same azimuthal location. Unfortunately, it was not possible to quantitatively measure the effect of this disturbance on the probe response but it was clear visually that the bow wave is small compared to films thicker than 1 mm.

The resistance of an ionic fluid is a strong function of the frequency of the applied signal. Braunstein & Robbins (1971) presented a thorough review of this phenomenon. Coney (1973) and Brown *et al.* (1978) addressed the more practical aspects associated with the choice of a carrier frequency for the probe. Brown *et al.* determined that a carrier frequency in excess of 50 kHz is optimal.

In most experiments it is impossible to prevent some variation of liquid conductivity with time. In particular, dissolved gasses can cause slow changes in conductivity. To overcome this problem the conductivity of the liquid was measured by a reference probe located in the upstream liquid supply line. The reference probe uses the same circuit as the thickness probe, but the circuit is connected to a constant geometry test cell. This cell is constructed so that the geometry of the liquid between the wires is independent of flow rate or other conditions of the film. The output of the reference probe therefore varies only with the conductivity of the liquid. The output of the thickness probe is non-dimensionalized by dividing it by the output of the reference probe. Once a thickness probe is calibrated to relate the dimensionless output to film thickness, the conductivity of the liquid is eliminated as a variable.

4. PROTOTYPE CONSTRUCTION

The electronic circuitry for the probe is shown schematically in figure 2. The carrier frequency is produced by an external sine wave oscillator. The carrier input is buffered by the first operational amplifier to decouple the input impedance from the load impedance of the probe. The probe wires are electrically isolated by magnetic coupling to prevent the formation of ground loop currents and currents between adjacent probes. Since the carrier is modulated by a varying resistance, the current through the probe, rather than the voltage drop across it varies linearly with the film thickness. The first stage of the detection circuit therefore converts the current signal to a voltage signal. The voltage is then applied to a full-wave rectifier to obtain a d.c. voltage. The carrier signal is rejected by a second-order low-pass filter set at 10 kHz. The 10 kHz cutoff allows adequate removal of the 100 kHz carrier frequency without introducing significant distortion into any signal components < 1 kHz.

Since the theoretical conductivity model has inherent limitations, a static test was performed to determine the linearity of the probe. Figure 3 shows the equipment used for this test. Platinum–rhodium alloy wires were mounted vertically in a stationary liquid reservoir. The 0.08 mm wires were mounted on 0.51 mm center spacing and were approx. 60 mm in length. The wire diameter chosen was the smallest commercially-available wire that had sufficient strength to resist breakage. As can be seen from figure 1, the smallest possible wire spacing gives the best spatial resolution. For this prototype, the center spacing was the smallest spacing that could be machined

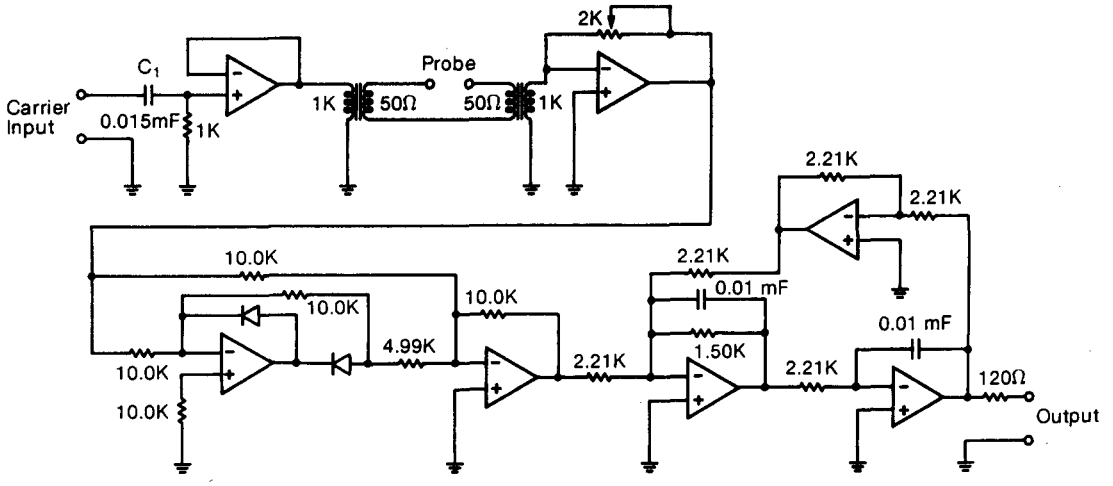

Figure 2. Schematic diagram of the probe electronics.

practically. According to figure 1, the spatial resolution of the probe based on 95% total resistance was 1.1 mm in the y-direction and 1.5 mm in the x-direction.

To calibrate this prototype, the depth of the liquid in the reservoir was measured with a micrometer and the output of the thickness probe was measured for each depth. Figure 4 shows that the dimensionless probe output varied linearly with film thickness over the range 0–12 mm.

Ideally, liquid electrical conductivity is eliminated as a variable from calibration plots so that they can be used for any liquid regardless of its properties. In practice, however, it is important to properly interpret the non-linear part of the plot. The calibration becomes non-linear when the electrical resistance between the wires is not much larger than the resistance of the wires themselves. If the value of the conductivity of the liquid increases, the magnitude of the resistance between the wires will decrease for any given film thickness. Since the resistance of the wires remains constant, non-linearity of the probe output becomes relatively more significant as the liquid conductivity increases, and the linear range of the calibration curve becomes smaller. Conversely, if the liquid conductivity decreases, the linearity of the calibration curve improves. Therefore, a linear calibration curve generated with one liquid may be used with confidence for any liquid with lower conductivity, but must be verified for liquids with higher conductivity.

Figure 5 shows a typical installation of a probe mounted on a vertical cylindrical column. The wires were secured to the column by passing them through holes drilled in the column wall and

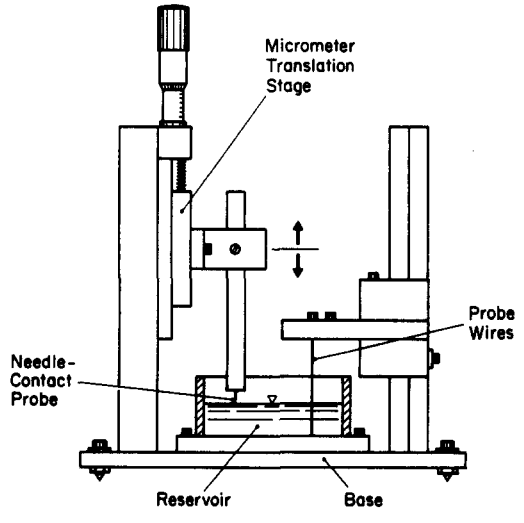

Figure 3. Static test cell for probe calibration

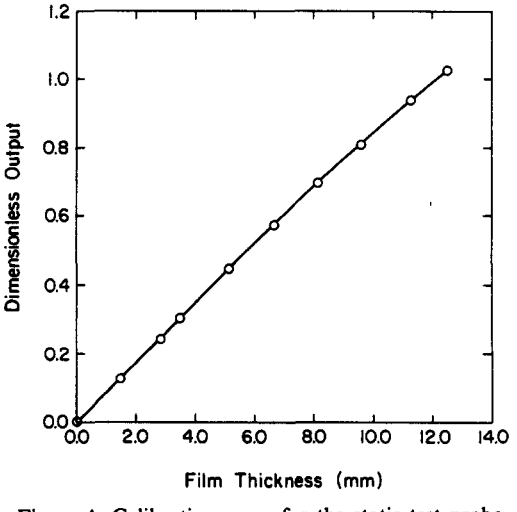

Figure 4. Calibration curve for the static test probe.

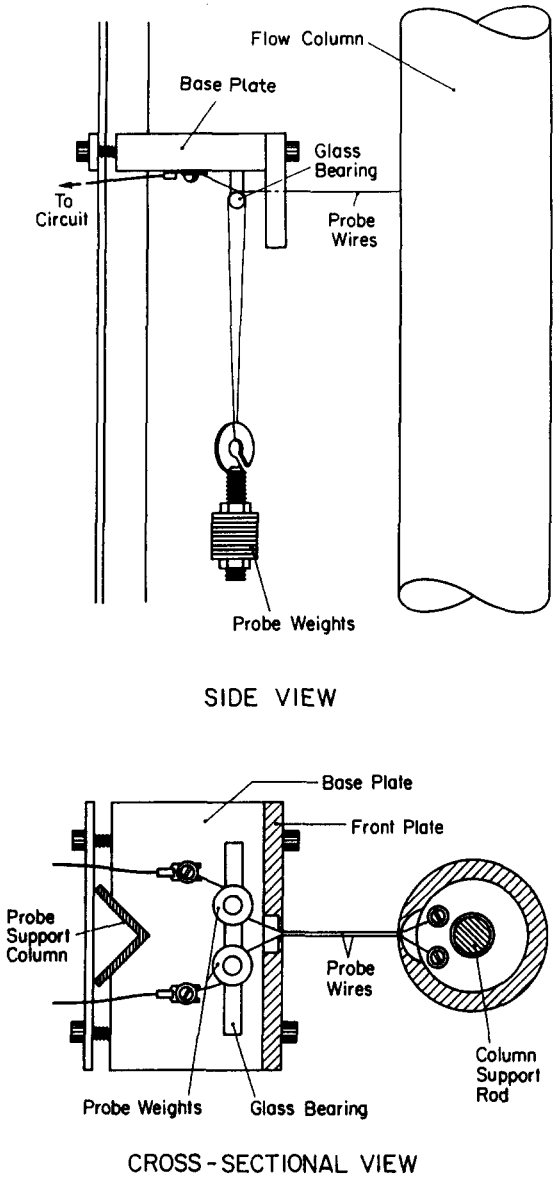

Figure 5. Typical installation of the probe on a vertical cylindrical column.

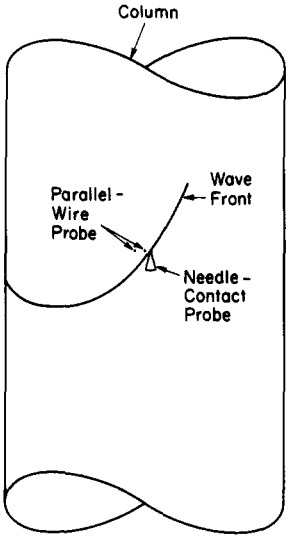

Figure 6. Schematic of a skewed wave front.

by anchoring each with a screw. They proceed horizontally outward from the cylinder, and each pair lies in a single horizontal plane. Outside the film, the wires were positioned by passing each through a small hole in a rigidly mounted vertical plate from which they were maintained in tension by weights.

The spacing of the wires was so close that tolerances in drilling the mounting holes could cause significant variation in the slope of the calibration curves of the prototype static probe and that of an actual probe on the column. Thus, calibration was performed to determine the exact geometry of each probe after it was installed. A needle-contact probe was used to trigger data collection when the film attained the thickness at which the needle was positioned. The needle-contact probe consisted of a needle which was translated by a micrometer so that it was held a measured distance from the film. This needle was positioned at the same horizontal plane as the wires and was always < 1 mm from the wires. The electronic circuitry generated a trigger pulse at the instant the needle first touched liquid. The output of the parallel-wire probe was recorded for times before and after the trigger so that the form of the triggering wave could be observed.

Like all transducers, the probe has a finite frequency response. This limit prevents accurate measurement of the front of steep wave fronts. Brown *et al.* (1978) analyzed the response of a parallel-wire probe to a square wave that has an infinite spanwise extent. Their model predicts the ratio of the actual probe output for a square wave of given streamwise length and arbitrary height to the output of the probe for an infinitely long film of the same thickness. This ratio was computed for all positions along the square wave. The square wave is an approximation to the front of a large wave on a vertical wall. Application of the theory of Brown *et al.* to the present probe suggests that a square wave of length $\gtrsim 2.5$ mm will not be resolved to within 5% accuracy until 0.5 mm of the wavelength has passed the probe. Shorter square waves will not be resolved to 5% accuracy. This result suggests that a wave which crests in a vertical distance of < 0.5 mm will not be properly resolved. The wave will appear to have a rounded front. Occurrence of this error during calibration with a needle-contact probe will always result in the parallel-wire probe indicating a wave height that is the same or less than the needle probe.

Variations in the azimuthal, or spanwise, direction presents a further complication to the comparison between measurements made with the two types of probes. Near the edge of a wave, the front of the wave may be skewed so that it forms a significant angle with the vertical direction. Flow visualization indicated that this general wave shape is very common in the Re range of $4\Gamma/\nu = 1000$–$75{,}000$, where Γ and ν are the volumetric flow rate per unit length normal to the flow direction and the kinematic viscosity, respectively. In this case, illustrated schematically in figure 6, the crest of the wave will touch one of the probes before it contacts the other. The height indicated by the wire probe can be either higher or lower than that indicated by the needle probe. Because the azimuthal location of a wave on the column is apparently random, it is expected that the distribution of this error will be symmetric about the correct calibration.

High-speed motion pictures of wave profiles showed that some waves on a vertical free-falling liquid film have fronts which fold over themselves. The resulting front looked very much like the front of a breaking ocean wave. Figure 7 qualitatively compares folding and non-folding waves. The needle-contact probe and the present probe reacted differently to such a wave front. The needle-contact probe recorded only the peak value of the wave height regardless of any folding. The present probe recorded only the wetted length of the wires. Therefore, if the wave front folded, the needle-contact probe recorded a higher peak than did the parallel-wire probe.

Each calibration datum point was acquired by moving the needle probe from outside the film until it touched a single wave. Therefore, data collection tended to occur at the peaks of waves. These points were plotted as shown in Figure 8. A calibration curve was hand fit to the highest data points. This curve was chosen with the assumption that the major calibration errors are the limited spatial frequency response of the wire probe and the folding wave fronts. The error caused by skewed wave fronts was neglected because it was assumed that the close placement of the probes would limit this error.

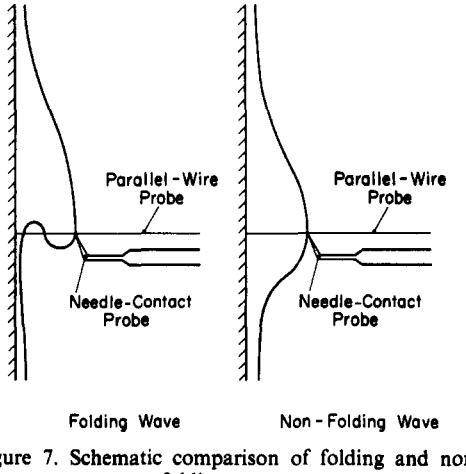

Figure 7. Schematic comparison of folding and non-folding waves.

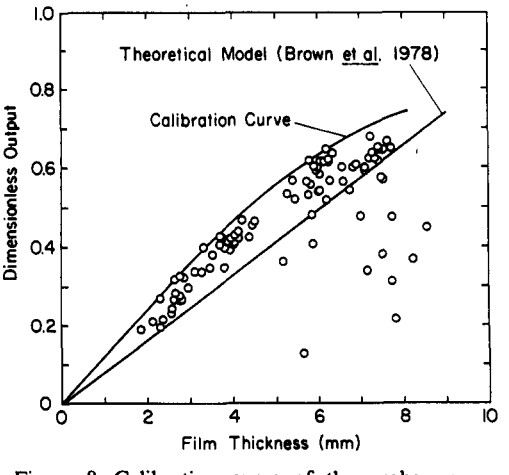

Figure 8. Calibration curve of the probe on a vertical cylindrical column.

The theoretical calibration curve for the probe using equations for the probe resistance given by Brown *et al.* (1978) is also shown in figure 8. This curve is described by the relationship

$$\frac{G_p}{G_R} = \frac{h \ln\left(\frac{b_R}{d_R}\right)}{\ln\left(\frac{b_p}{d_p}\right)},$$

where G is the conductance, b is half the wire spacing, and d is the wire diameter. The subscript p refers to the measurement probe and R to the reference. It is apparent that calibration was necessary to determine the effect of actual probe geometry. It can also be seen that some non-linearity exists in the calibration. This non-linearity was probably due to a combination of non-parallel wires and electrical resistance in the wires and leads.

The wave folding phenomena is an inherent problem for all existing film thickness probes, including the present one. No single probe accurately resolves the shape of a folding wave front. However, flow visualization of the film profile indicated that while these wave fronts exist, they affect the probe for extremely short time periods and showed that folding waves are a small percentage of the total. This flow visualization was performed with water films over the Re range 1000–75,000 and with water–propylene glycol mixtures over the Re range 100–5000. The largest number of folding waves in a given time record was approx. 10% of the total number of waves detected. In this worst case, the ratio of the time during which the folding part of the wave passed the measurement point to the total time record was <0.0001. The error introduced in statistical properties of the film thickness by not properly resolving the folding wave fronts is negligible except for statistics which apply to the wave fronts alone.

The probe was installed in a flow loop which included a vertical column 0.050 m dia and 2.13 m long. A liquid film was formed on the outside of the column by injection through a porous tubular section at the top of the column. This apparatus is described in the thesis of Koskie (1987).

In order to verify the method of calibration of the wire probe, mean film thickness data were taken with a needle-contact probe. These data were taken with water, 1.913 m downstream of the porous section, and at Re values of 4200, 17,600 and 61,300. The resulting values of mean film thickness taken by each method are compared in Figure 9. The error bounds on the needle-contact probe reflect an estimated 95% confidence of 0.13 mm in the position of the tip of the needle relative to the wall. The mean film thickness indicated by each probe agree well for the low and high film rates. They differ by 19% at the middle flow rate. Additional tests with each probe showed that the respective mean thicknesses were repeatable. It is therefore assumed that the errors involving each measurement happened to be additive in this case. The true thickness is probably between these. An alternate calibration curve was proposed which fit a least-squares second-order polynomial to selected data. This method did not result in improved agreement with the needle-contact data. The calibration curve used was therefore assumed to be the best possible fit.

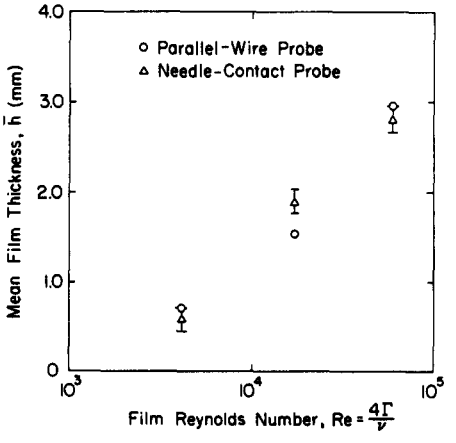

Figure 9. Comparison of mean film thickness taken by needle-contact and parallel-wire probes.

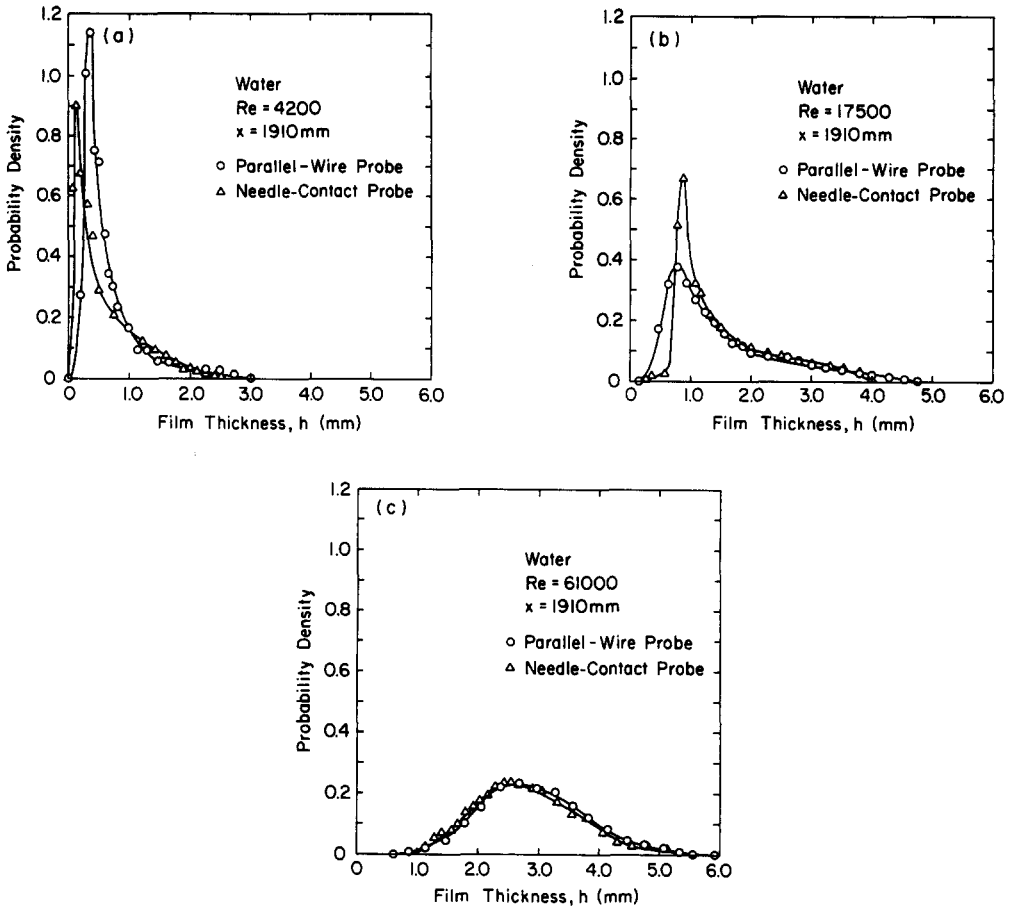

Figure 10. Comparison of thickness probability density functions for needle-contact and parallel-wire data.

Figure 10 compares the probability density functions for thickness measurements taken by each probe. The distributions show very good agreement at thicknesses >1 mm. The major differences occur at smaller thicknesses in regions where the slope of the probability function is very large. This observation suggests that the wire probe provides excellent accuracy for thick films. It is unclear whether the needle-contact probe, the wire probe or the combination of both produces the

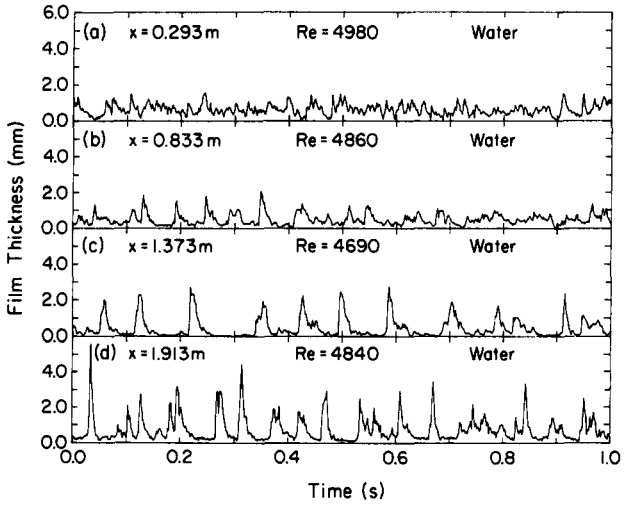

Figure 11. Output of the film thickness probe for a water film in the Re range 4690–4980 at distances of (a) 0.293 m, (b) 0.833 m, (c) 1.373 m and (d) 1.913 m from the top of the column.

discrepancies observed at small thickness. The parallel-wire probe has a distinct advantage over the needle-contact probe because it provides time-resolved film thickness data. This type of data is necessary for autocorrelation data and studies of wave shapes.

Typical output records of the parallel-wire film thickness probe are shown in figure 11. These figures demonstrate the wide variation in flow pattern observed with falling liquid films. All the data shown were obtained an Re of approx. 5000. Figure 11 shows the thickness of a water film as a function of time at four locations on the column. These locations were (a) 0.293 m, (b) 0.833 m, (c) 1.373 m and (d) 1.913 m from the top of the column.

The most striking observation that can be made from these plots is the wide variation in wave shape and amplitude at fairly similar Re. Figure 11 shows that both the amplitude and shape of the waves on a water film change with distance. This observation is consistent with the previous work of Salazar & Marschall (1978) and Portalski & Clegg (1972). More of these data are presented in Koskie (1987).

5. CONCLUSIONS

The spatial resolution and frequency response of parallel-wire film thickness probes can be improved by decreasing the physical dimensions of the probe. A method has been presented for calibrating parallel-wire probes which are sufficiently small that machining tolerances can cause significant errors. The calibrated parallel-wire probe yields continuous thickness measurements for thick films.

Waves with folding fronts were discovered on vertically-falling liquid films. The fronts of these waves are similar in appearance to breaking ocean waves. While the probe cannot fully resolve these folding wave fronts, this phenomenon is insignificant for film statistics such as time-averaged film thickness.

Acknowledgement—This work was supported by the U.S. Department of Energy, Office of Basic Sciences under DOE Grant No. DE-FGO2-85ER13398.

REFERENCES

BRAUNSTEIN, J. & ROBBINS, G. D. 1971 Electrolytic conductance measurements and capacitive balance. *J. Chem. Educ.* **48,** 52–59.

BROWN, R. C., ANDREUSSI, P. & ZANELLI, S. 1978 The use of wire probes for measurement of liquid film thickness in annular gas–liquid flows. *Can. J. Chem.* **56,** 754–757.

CONEY, M. W. E. 1973 The theory and application of conductance probes for the measurement of liquid film thickness in two-phase flow. *J. Phys. E: Scient. Instrum.* **6,** 903–910.

DAILY, J. W. & HARLEMAN, D. R. F. 1966 *Fluid Dynamics*, p. 381. Addison-Wesley, Reading, Mass.

HEWITT, G. F. 1978 *Measurement of Two Phase Flow Parameters*, pp. 177–179. Academic Press, London.

JACKSON, J. D. 1975 *Classical Electrodynamics*, 2nd edn, p. 244. Wiley, New York.

KOSKIE, J. E. 1987 Interfacial characteristics of falling liquid films. MSME Thesis, Purdue Univ. West Lafayette, Ind.

MIYA, M., WOODMANSEE, D. E. & HANRATTY, T. J. 1971 A model of roll waves in gas–liquid flow. *Chem. Engng Sci.* **26,** 1915–1931.

PORTALSKI, S. & CLEGG, A. J. 1972 An experimental study of wave inception on falling liquid films. *Chem. Engng Sci.* **27,** 1257–1265.

SALAZAR, R. P. & MARSCHALL, E. 1978. Time average local thickness measurement in falling liquid film flow. *Int. J. Multiphase Flow* **4,** 408–412.

SWANSON, R. W. 1966 Characteristics of the gas–liquid interface in two phase annular flow. Ph.D. Thesis, Univ. of Delaware, Delaware.